

The influence of climate regime shift on ENSO

Zhengqing Ye and William W. Hsieh

Dept. of Earth and Ocean Sciences, University of British Columbia

Vancouver, B.C. V6T 1Z4, Canada

submitted to *Climate Dynamics*

(revised)

8th December 2005

Corresponding author:

Zhengqing Ye, Dept. of Earth and Ocean Sciences, University of British Columbia, 6339 Stores Road, Vancouver, B.C. V6T 1Z4, Canada

Tel: +1-604-8225691, Fax: +1-604-8226088, Email: zye@eos.ubc.ca

Abstract

Observations indicated that for the El Niño/Southern Oscillation (ENSO) there have been eastward displacements of the zonal wind stress anomalies and surface heat flux (short wave heat flux and latent heat flux) anomalies during El Niño episodes in the 1981-1995 regime relative to the earlier regime of 1961-1975 (without corresponding displacements during La Niña episodes). Our numerical experiments with the Zebiak-Cane coupled model generally reproduced such displacements when the model climatological fields were replaced by the observed climatologies (of sea surface temperature, surface wind and associated atmospheric divergence) and simulated climatologies (of oceanic surface layer currents and associated upwelling) for the 1981-1995 regime. Sensitivity tests indicated that the background atmospheric state played a much more important role than the background ocean state in producing the displacements, which enhanced the asymmetry between El Niño and La Niña in the later regime. The later regime climatology state resulted in the eastward shifts in the ENSO system (wind stress and sea surface temperature) only during El Niño, through the eastward shift of the atmosphere convergence heating rate in the coupled model. The ENSO period and ENSO predictability were also enhanced in the coupled model under the later regime climatology. That the change in the mean state of the tropical Pacific atmosphere and ocean after the mid 1970s could have produced the observed changes in ENSO properties is consistent with our findings.

1 Introduction

The characteristics of the El Niño/Southern Oscillation (ENSO) have experienced an abrupt change or ‘regime shift’ in the mid 1970s, which is usually attributed to the decadal/interdecadal climate variability in the Pacific Ocean (Zhang et al, 1997, Wang and An, 2001). Recent studies (McPhanden and Zhang, 2004) found that the Pacific Ocean has rebounded since 1998, where the rebound can be viewed as an opposite shift relative to the shift in the mid 1970s. There is no consensus on the fundamental dynamics of ENSO decadal variability. Some modeling results

suggested that the decadal variability in the tropical Pacific originates from mid-latitude variability (Latif and Barnett, 1996), while others proposed it comes from tropical internal nonlinear instability (Knutson and Manabe, 1998) or uncoupled atmospheric noise (Thompson and Battisti, 2001; Flügel et al, 2004). Two hypotheses have been proposed to explain the linkage between the extratropical decadal variability and the tropical decadal variability, one by an oceanic teleconnection pathway (Gu and Philander, 1997; Kleeman et al, 1999), the other by an atmospheric bridge (Barnett et al, 1999).

Since a decadal/interdecadal change in the tropical Pacific amounts to a change in the background mean state for the ENSO phenomenon, how the background state affects ENSO properties has become an area of active investigation. Studies have shown that changes in the background state would alter ENSO in period, intensity, direction of propagation and spatial structure. For instance, Fedorov and Philander (2001) studied theoretically the changes in ENSO properties caused by background changes in the wind stress intensity, thermocline depth and temperature difference across the thermocline, and concluded that the observed ENSO property changes since the 1960s are consistent with their theory. Wang and An (2002) proposed that the changes in the background winds and the corresponding ocean dynamic fields played the dominant role on the abrupt change in ENSO properties since the late 1970s. A caveat is that the periods used to calculate the mean states are relatively short, and the presence of an extra El Niño or a very strong El Niño during a particular decadal period could introduce a difference in the calculated mean states, i.e. the mean decadal states are themselves influenced by ENSO episodes.

Recently, the nonlinearity and asymmetry of decadal variability in the tropical Pacific were recognized (Rodgers, 2004). Jin et al (2003) suggested that the nonlinear dynamic heating in the tropical Pacific ocean heat budget is essential in generating the nonlinearity and asymmetry of decadal ENSO. Changes in the asymmetry and nonlinearity of ENSO over different climate

regimes have also been studied. Wu and Hsieh (2003) found that the leading nonlinear canonical correlation analysis (NLCCA) mode between the tropical Pacific sea surface temperature (SST) and wind stress (WS) showed that after the climate regime shift of the mid 1970s, there was an eastward shift in the westerly anomalies during warm ENSO episodes, but no shift in the easterly anomalies during the cold ENSO episodes, thereby enhancing the asymmetry between El Niño and La Niña in the post-shift regime compared to the pre-shift regime. ENSO predictability has been found to be higher during the decades when the ENSO asymmetry is large (An, 2004).

In this paper, by analyzing a coupled model of intermediate complexity and observed data, we investigated how changes in the background climate state affect properties of ENSO, especially the asymmetry between El Niño and La Niña, zonal shifts in the observed net shortwave radiation flux and latent heat flux, shifts in the model convergent heating rate, and ENSO predictability. This paper is organized as follows: In section 2, we introduce the datasets, the nonlinear data analysis method and the coupled model. In section 3, observed data are first analyzed for the ‘regime shift’ in the asymmetry of ENSO, then the intermediate coupled model is run to see how different background states (of surface wind, heat fluxes, and sea surface temperatures) change the ENSO properties. A discussion follows in section 4.

2 Data and methods

2.1 Data

National Oceanic and Atmospheric Administration (NOAA) extended reconstructed SST was used in this study. The extended reconstructed sea surface temperature (ERSST) was constructed using the most recently available international comprehensive ocean-atmosphere data set (ICOADS) SST data and improved statistical methods that allow stable reconstruction using

sparse data. This monthly analysis begins January 1854, but because of sparse data the analyzed signal is heavily damped before 1880 (Smith and Reynolds, 2004). The monthly WS was objectively analyzed at the Florida State University (Bourassa et al, 2001), while the sea surface heat flux data is from da Silva et al (1994) (which terminated after 1993). The climatological monthly mean is removed from the data to obtain the monthly anomaly.

2.2 Nonlinear principal component analysis

For the time series data $\mathbf{x}(t) = [x_1, \dots, x_l]$, where each variable x_i is a time series containing n observations, the principal components analysis (PCA) method looks for u , a linear combination of the x_i , and an associated vector \mathbf{a} , with

$$u(t) = \mathbf{a} \cdot \mathbf{x}(t)$$

so that

$$J = \langle \|\mathbf{x}(t) - \mathbf{a}u(t)\|^2 \rangle$$

is minimized. Here $\langle \dots \rangle$ denotes a sample or time mean, u , the first principal component (PC), is a time series, while \mathbf{a} , the first empirical orthogonal function (EOF), describes a spatial pattern.

The fundamental difference between nonlinear principal components analysis (NLPCA) and PCA is that NLPCA allows a nonlinear mapping from \mathbf{x} to u and a nonlinear inverse mapping from u to \mathbf{x}' , whereas PCA only allows linear mapping (Kramer, 1991; Hsieh, 2004). For NLPCA,

$$u = F(\mathbf{x}), \quad \mathbf{x}' = \mathbf{G}(u),$$

where F and \mathbf{G} denote the nonlinear mapping and inverse mapping functions respectively (Fig. 1).

The NLPCA method is used to analyze the nonlinear modes of SST and WS in the tropical Pacific. Prior to NLPCA, combined PCA, also called combined EOF analysis, is performed on the

SST and WS anomalies, i.e., we performed PCA analysis on the combined field of SST anomalies and WS anomalies, with each variable first normalized by its standard deviation. Then, the leading 6 PCs are used as the inputs to the NLPCA model.

2.3 Coupled model

The coupled model is based on the Zebiak-Cane model (Zebiak and Cane, 1987), where the atmospheric component consists of steady-state, linear shallow-water equations on an equatorial beta plane with a nonlinear convergence feedback, while the oceanic component is a linear reduced-gravity model. With a time step of (about) 10 days, the ocean model domain covers the tropical Pacific from 29°S to 29°N, and from 124°E to 80°W, where the grid for ocean dynamics is 2° longitude by 0.5° latitude, and the grid for SST physics and the atmospheric model is 5.625° longitude by 2° latitude.

The temperature equation for the surface layer follows Zebiak and Cane (1987):

$$\begin{aligned} \frac{\partial T}{\partial t} = & -\mathbf{u}_1 \cdot \nabla(\bar{T} + T) - \bar{\mathbf{u}}_1 \cdot \nabla T - \{M(\bar{w}_s + w_s) - M(\bar{w}_s)\} \times \frac{\partial \bar{T}}{\partial z} - M(\bar{w}_s + w_s) \frac{T - T_e}{H_1} - \alpha_s T \\ & - K_t \frac{T - T_e}{H_1} + A_h \Delta_h T, \end{aligned} \quad (1)$$

where we have added the last two terms to simulate vertical mixing and horizontal diffusion in the temperature equation (Boulangier and Menkes, 2001). Here $\bar{\mathbf{u}}_1(x, y, t)$ and $\bar{w}_s(x, y, t)$ are the prescribed climatological monthly mean horizontal current and upwelling in the surface layer respectively, $\bar{T}(x, y, t)$ is the prescribed mean SST, $\partial \bar{T}(x)/\partial z$ the prescribed mean vertical temperature gradient, the mean surface layer depth $H_1 = 50$ m, the diffusion coefficient $\alpha_s = (125 \text{ day})^{-1}$, $K_t = 2.5 \times 10^{-5} \text{ m s}^{-1}$, $A_h = 2000 \text{ m}^2 \text{ s}^{-1}$, the function M is defined by

$$M(x) = \begin{cases} 0, & x \leq 0 \\ x, & x > 0, \end{cases} \quad (2)$$

and the entrainment velocity is

$$w_s = H_1 \left(\frac{\partial u_1}{\partial x} + \frac{\partial v_1}{\partial y} \right). \quad (3)$$

The entrainment temperature anomaly, T_e , is given by

$$T_e = \gamma T_{\text{sub}} + (1 - \gamma)T, \quad (4)$$

where T_{sub} originally has the empirical parameterization form (Zebiak and Cane, 1987) :

$$T_{\text{sub}} = \begin{cases} T_1 \left\{ \tanh[b_1(\bar{h} + h)] - \tanh(b_1\bar{h}) \right\}, & h > 0 \\ T_2 \left\{ \tanh[b_2(\bar{h} - h)] - \tanh(b_2\bar{h}) \right\}, & h < 0 \end{cases} \quad (5)$$

with $\bar{h}(x)$ the prescribed mean upper layer depth, $\gamma = 0.75$, $T_1 = 28^\circ\text{C}$, $T_2 = -40^\circ\text{C}$, $b_1 = (80 \text{ m})^{-1}$ and $b_2 = (33 \text{ m})^{-1}$.

Here instead, an empirical parameterization scheme was developed to estimate T_{sub} in terms of other ocean dynamical variables in the temperature equation (1). With the ocean model forced by the observed WS during 1964-1998, T_{sub} was inversely calculated from the temperature equation (1) using the observed SST for T and the model anomalous currents (Zhang et al, 2005). PCA was separately applied to the simulated upper layer depth anomalies h , and to T_{sub} to extract the leading PCs . The nonlinear regression relationships between the first three PCs of h (the predictors) and the first three PCs of T_{sub} (the predictands) were obtained by a neural network method (Tang and Hsieh, 2002; Li et al, 2005). Then the nonlinear regression relationships were used to replace equation (5) in the coupled model. This new parameterization has corrected the original coupled model bias where the variances (for both temperature and WS) were unrealistically confined to the eastern tropical Pacific, as the new simulated subsurface temperature anomalies extend to central equatorial Pacific (not shown). Nonlinear relations between the leading PCs of T_{sub} and those of h can be seen in Fig. 2 .

3 Results

3.1 Observational results

A shift in the ENSO properties, both atmospheric and oceanic, occurred in the mid 1970s (Zhang et al, 1997; An and Wang, 2000). Decadal differences in the SST and the surface WS field were calculated by subtracting the 1961-1975 mean from the 1981-1995 mean (Fig. 3). In the SST field (Fig. 3a), the decadal difference exhibits an ENSO-like pattern over the tropical Pacific. In the WS field, there are decadal westerly anomalies over the western equatorial Pacific and easterly anomalies over the eastern equatorial Pacific, resulting in a convergence region in the central equatorial Pacific (Fig. 3b).

Next, the NLPCA method was applied to analyze the observed tropical Pacific SST anomaly and WS anomaly during the 1961-1975 regime, and separately, the 1981-1995 regime. The 6 leading PCs of the combined PCA of the SST field and WS field were used as the inputs to the NLPCA model. Results show that there exists an eastward spatial shift by over 15° in the westerly WS anomaly field (associated with El Niño episodes) in the central equatorial Pacific in 1981-1995 regime (Fig. 4c) compared to that in 1961-1975 regime (Fig. 4a). However, there is no significant zonal shift in the easterly WS anomaly field (associated with La Niña) in the central equatorial Pacific between the two regimes (Figs. 4b and d). The amplitudes of both westerly and easterly WS were intensified during the 1981-1995 regime. These results are similar to the results found by using NLCCA on SST and WS fields in the 1961-1975 and 1981-1999 regimes (Wu and Hsieh, 2003).

The surface heat fluxes are also analyzed using the NLPCA. The 6 leading PCs of the combined PCA of the SST, net shortwave radiation and latent heat flux fields (with each field variable normalized by its standard deviation) are used as the inputs to the NLPCA model. Similar

eastward shifts (associated with El Niño episodes) can be seen in the net shortwave radiation field and, to a lesser extent, in the latent heat flux field in the later regime compared to the earlier regime. (Fig. 5). The eastward shift of the net shortwave radiation is the result of eastward shift of tropical clouds over the Pacific during El Niño episodes in the later regime. Similar shifts are also found in the composite maps of the net shortwave radiation field or the latent heat flux field for El Niño episodes (not shown). Hence the net shortwave radiation and latent heat flux fields together with the SST and zonal WS displayed greater asymmetry between El Niño and La Niña during the later regime as a result of the eastward shift in the anomalies during El Niño but not during La Niña. However, similar analyses on the net longwave radiation field and the sensible heat flux field did not reveal significant shifts in the later regime (not shown).

3.2 Model simulation results

The Zebiak-Cane coupled model, with the new subsurface temperature parameterization by neural networks, is used to study the influence of the climate shift in the mid 1970s on ENSO properties. In this model, the background seasonal climatology is prescribed, and can be changed for different climate regimes. Five sets of experiments were performed in this study.

The first set (set A) replaced the model oceanic monthly climatological fields (SST, oceanic surface layer currents and associated upwelling/downwelling) and the atmospheric climatologies (monthly surface WS fields and monthly surface wind divergence fields) with specified data for the 1961-1975 regime and the 1981-1995 regime in two separate model runs. Among these prescribed monthly climatological fields, the surface WS, surface wind divergence and SST were observed data, while the oceanic surface layer currents and associated upwelling/downwelling were computed for the two regimes from a run of the Zebiak-Cane ocean model forced by the observed WS during 1961-1995. Set B prescribed, in separate runs, the atmospheric monthly climatologies for

the two regimes (but retained the original ocean climatologies), while set C prescribed the oceanic monthly climatologies for the two regimes (but retained the original atmospheric climatologies). Although the atmospheric and oceanic climatologies are in reality coupled, these additional sets try to identify the separate effects of changing the background state of the atmosphere and the ocean. Set D was similar to set A except that the oceanic monthly climatologies of the 1961-1975 regime were exchanged with that of the 1981-1995 regime, i.e., the model was prescribed with the atmospheric climatologies from the 1961-1975 regime and the oceanic climatologies from the 1981-1995 regime in D1, while in D2, the 1981-1995 atmospheric climatologies were paired with the 1961-1975 oceanic climatologies. Recent studies (McPhaden and Zhang, 2005) showed that Pacific Ocean circulation rebounded between July 1992-June 1998 and July 1998- June 2003, resulting in anomalously cool tropical Pacific SST during the period 1998-2003. This rebound can be viewed as an opposite shift relative to the shift in the mid 1970s. To study the effects of this opposite shift, set E used the atmospheric and oceanic monthly climatologies from the July 1992-June 1998 regime and the July 1998-June 2003 regime in two separate runs. For each experiment, the coupled model was run for 300 years and the statistical behavior of the model ENSO was examined using the model output from the last 200 years.

The NLPCA was applied to SST and WS anomalies from set A to study the combined effect of the atmospheric climatology and the oceanic climatology in the 1961-1975 regime and in the 1981-1995 regime. Fig. 6 shows that for strong El Niño the center of the SST anomalies (defined by the maximum value of the anomalies, as marked by the “H” in Fig. 6e) under the 1981-1995 regime climatology had an eastward displacement of about 11° relative to that under the 1961-1975 regime climatology (as marked by the “H” in Fig. 6a). In contrast, the center of the SST anomalies corresponding to strong La Niña did not show zonal displacement after the regime shift (as indicated by the location of the two “L” in Figs. 6c and g). There is evidence for a

displacement in the zonal location of the westerly WS anomaly centers as well. During strong El Niño, the westerly WS anomalies for the case using the 1981-1995 regime climatologies (Fig. 6f) were also enhanced in the eastern equatorial Pacific and the anomaly center shifted eastward by over 11° compared to that of the earlier regime (Fig. 6b). During strong La Niña, easterly anomaly WS centers were at similar zonal locations for both cases (Figs. 6d and h). Though the extents of the eastward shifts in the SST and WS anomaly centers during strong El Niño were somewhat weaker in our experiments than in the observed data (Fig. 4), they indicated enhanced asymmetry between El Niño and La Niña after the regime shift.

Table 1 summarizes the amount of eastward shift in the SST and zonal WS anomaly centers in the post-shift regime (relative to those in the pre-shift regime) during strong El Niño and during strong La Niña, as determined from NLPCA. In the B experiments where the atmospheric climatologies for the two regimes were prescribed, during strong El Niño, the westerly WS anomaly center shifted eastward by 11° in the later regime (relative to the earlier regime), while the SST anomaly center was displaced by only 6° eastward. During strong La Niña, neither the easterly WS anomaly center nor the cool SST anomaly center was displaced after the regime shift (Table 1).

In the C experiments where the oceanic climatologies for the two regimes were prescribed, during strong El Niño, the zonal WS anomaly center showed weaker displacement compared to experiments A and B, while the SST anomaly center shifted eastward by 6° after the regime shift. Again, during strong La Niña no displacement in the zonal WS and SST anomaly centers can be found after the regime shift (Table 1). A caveat is that as the prescribed oceanic climatology was calculated from an ocean model driven by atmospheric forcing, it is not totally unaffected by the atmospheric climatology. The D experiments will show that this “indirect atmospheric climatology effect” through the oceanic climatology is minor.

In the D experiments, where D1 has the 1961-1975 atmospheric climatology and the 1981-1995 oceanic climatology prescribed, and D2 the 1981-1995 atmospheric climatology paired with the 1961-1975 oceanic climatology, during strong El Niño the westerly center shifted eastward by 11° in D2 relative to D1 (Table 1), demonstrating that the atmospheric climatology was primarily responsible for the eastward shift of the westerly WS anomaly. Also these mixed climatology experiments showed that the “indirect atmospheric climatology effect” through the oceanic climatology is minor— if this indirect effect were as strong as the direct effect, then we would see no shift in the WS and SST anomaly centers between D2 and D1, as the the 1981-1995 atmospheric climatology would exert its direct effect in D2 and its indirect effect (via the oceanic climatology) in D1.

The E experiments (Table 1) showed that opposite zonal shifts in the WS and SST anomaly centers can be produced by the rebound mean state. Hence the WS and SST anomaly shifts during strong El Niño induced by a change in the mean state are actually reversible, allowing both eastward and westward shifts to occur. However, throughout experiments A to E, the changes in the mean state did not induce shifts in the WS and SST anomaly centers during La Niña.

We also tested the sensitivity of T_{sub} parameterization based on data from the ocean model forced by the observed wind stress before and after the mid 1970s. The nonlinear regression relationships were derived from the pre- and post-shift regimes separately. Westerly anomaly shifts similar to those seen in set A were found regardless whether the T_{sub} parameterization were derived from the periods 1964-75, 1981-95 or from the longer period of 1964-98. Thus the westerly anomaly shifts were caused by changes in the climatology rather than parameterization, thereby justifying our use of the single T_{sub} parameterization during the different regimes.

ENSO is an interactive thermodynamic system between the atmosphere and ocean, where the

atmosphere dynamically forces the ocean by the surface WS, while the ocean thermally affects the atmosphere by heating/cooling. In the Zebiak-Cane coupled model, there are two heating anomaly terms in the atmospheric model (see Zebiak and Cane, 1987): the surface heating rate (Q_s) due to the SST and the convergence heating rate (Q_c) due to the moisture procedure. In our set A experiments, NLPCA revealed that during strong El Niño, the Q_c anomaly center intensified strongly and shifted eastward by about 28° in the later regime (Fig. 7b) relative to the earlier regime (Fig. 7a), while no significant eastward shift was found for the Q_s field (not shown). During strong La Niña, shifts were found neither in the Q_c field nor in the Q_s field (not shown). Hence it appears that Q_c played a role in altering the atmospheric circulation during El Niño in the later regime. These model results are consistent with the observed eastward shifts in the shortwave radiation and latent heat flux anomalies (Fig. 5) and the absence of shifts in the longwave radiation and sensible heat flux anomalies in the later regime during strong El Niño, as the shortwave radiation and latent heat flux contributions would be grouped together under Q_c , and the longwave radiation and sensible heat flux under Q_s in the model.

Sensitivity experiments were also used to identify the impact of the heating rate Q_c . When the Q_c term was deleted in the coupled model for the A experiments, there were no WS westerly anomaly shifts in the later regime relative to the pre-shift regime. Thus the heating rate Q_c played a critical role in the WS westerly anomaly shift.

That ENSO predictability appeared to have changed following the mid 1970s regime shift has been pointed out by Chen et al (2004) and An (2005). We next compute the change in the potential predictability in our set A coupled model experiments. The average SST anomaly in the Niño 3.4 region was predicted at lead times from 0 to 12 months by linear regression models using the 6 leading SST anomaly PCs and 6 leading WS anomaly PCs as predictors. The cross-validated correlation coefficients between the predicted and actual Niño 3.4 indices from

our coupled model over 150 years can be used to represent potential predictability. Fig. 8 shows enhanced predictability in the post-shift climatology when the lead time is greater than 5 months. Fourier spectral analysis was also performed on the Niño 3.4 indices from the set A coupled model runs, where the spectral peak shifted from a period of 48 months under the pre-shift climatology to 52 months under the post-shift climatology (Fig. 9). Thus under the post-shift climatology, the ENSO mode has enhanced asymmetry between El Niño and La Niña (Fig. 6), increased ENSO period and enhanced potential predictability, relative to the earlier regime.

4 Discussion

Observations have revealed eastward shifts in the location of the zonal wind stress anomalies and the surface shortwave and latent heat flux during strong El Niño episodes after the mid 1970s climate regime shift. Using a modified Zebiak-Cane coupled model, we found that eastward shifts in the surface westerly anomalies and heating rate anomalies during the warm episodes were indeed found in the model when the 1981-1995 climatology was used instead of the 1961-1975 climatology. Our sensitivity studies indicated that it was mainly the change in the atmospheric climatology which caused the eastward shifts in the westerly anomalies and convergence heating rate anomalies, with the change in the upper ocean climatology being of minor importance. A caveat is that in the Zebiak-Cane model the most important climatology field affecting ENSO property is known to be the surface wind divergence (Tziperman et al, 1997), so perhaps our findings are due to the particular formulation used in this model. Indeed the strong shift found in the model convergence heating rate Q_c (which depends on the mean surface wind convergence), but not found in the surface heating rate Q_s (which depends on the mean surface temperature), may reflect the Zebiak-Cane model's formulation allowing stronger influence from the atmospheric climatology than from the oceanic climatology. However, the shift in the model Q_c being consistent

with the shift found in the observed shortwave radiation and latent heat flux, and the lack of shift in the model Q_s being consistent with the lack of shift in the observed long wave radiation and sensible heat flux suggest that the physics in the Zebiak-Cane model is correct, and that the stronger influence of the atmospheric climatology over the oceanic climatology in causing changes in ENSO may not be just an artifact of the model.

While the change in the surface background wind resulted in the eastward shifts in the surface wind anomalies and convergence heating rate anomalies during strong El Niño, during strong La Niña the eastward shifts were not evident in the 1981-1995 regime. Thus the asymmetry between the El Niño state and the La Niña state has been enhanced in the 1981-1995 regime, which also implies enhanced nonlinearity in the ENSO system. Also consistent with observations are the enhanced predictability and lengthened ENSO period found when the model was run with the 1981-1995 climatology. All these agreements with observations suggest that despite the uncertainties in using climatologies calculated from relatively short records, using the 1981-1995 climatology in the coupled model did induce changes in ENSO properties consistent with observed changes.

The presence of stronger or more El Niño episodes during the 1981-1995 regime could, through simple averaging, produce a change in the calculated SST mean state somewhat similar to that found (Fig. 3a). However, the change in the wind stress mean state (Fig. 3b) did not bear resemblance to the wind stress anomalies found during El Niño (Tang, 1995), so the change could not have been caused by the presence of stronger or more El Niño episodes during the 1981-1995 regime. One possibility is that the change in the wind stress mean state was transmitted into the tropics by the atmospheric bridge from the extratropics (Barnett et al, 1999).

Acknowledgements: We are grateful to Drs. A. Wu and S. Li for helpful discussions, and Dr. R.-H. Zhang for the valuable suggestion on the computation of the subsurface temperature. The Zebiak-Cane coupled model, developed originally by Drs. S.E. Zebiak and M.A. Cane, was kindly made available by the Lamont-Doherty Earth Observatory. This work was supported by the Canadian Foundation for Climate and Atmospheric Sciences, and the Natural Sciences and Engineering Research Council of Canada.

References

An S-I and Wang B (2000) Interdecadal change of the structure of the ENSO mode and its impact on the ENSO frequency. *J. Climate* 13:2044-2055

An S-I (2004) Interdecadal changes in the El Niño La-Niña asymmetry. *Geophys Res Lett*, 31:L23210. DOI:10.1029/2004GL021699

Barnett TP, Pierce DW, Latif M, Dommenges D and Saravanan R (1999) Interdecadal interactions between the tropics and midlatitudes in the Pacific basin. *Geophys Res Lett* 26(5):615-618. DOI:10.1029/1999GL900042

Boullanger J-P and Menkes C (2001) The Trident Pacific model. Part 2: role of long equatorial wave reflection on sea surface temperature anomalies during the 1993-1998 TOPEX/POSEIDON period. *Clim Dynam* 17:175-186

Bourassa MA, Smith SR and O'Brien JJ (2001) A new FSU winds and flux climatology. 11th Conference on Interactions of the Sea and Atmosphere. San Diego, CA, Amer Meteor Soc:912

Chen D, Cane MA, Kaplan A, Zebiak SE, and Huang D (2004) Predictability of El Niño in the past 148 years. *Nature* 428:733-736

- daSilva A, Young AC, and Levitus S (1994) Atlas of surface marine data 1994. Tech Rep 6, US Department of Commerce, NOAA, NESDIS
- Deser C, Phillips AS and Hurrell JW (2004) Pacific interdecadal climate variability: linkages between the Tropics and the North Pacific during boreal winter since 1900. *J Climate* 17:3109-3124
- Fedorov AV and Philander SGH (2001) A stability analysis of tropical Ocean- Atmosphere Interactions (Bridging Measurements of, and Theory for El Niño). *J Climate* 14:3086-3101
- Flügel, M, Chang P and Penland (2004) The role of stochastic forcing in modulating ENSO predictability. *J Climate* 17:3125-3140
- Gu D and Philander SGH (1997) Interdecadal climate fluctuations that depend on exchanges between the Tropics and extratropics. *Science* 275:805-807
- Hsieh WW (2004) Nonlinear multivariate and time series analysis by neural network methods. *Rev Geophys* 42(1):RG1003. DOI:10.1029/2002RG000112
- Jin F-F, An S-I, Timmermann A and Zhao J (2003) Strong El Niño events and nonlinear dynamical heating. *Geophys Res Lett* 30:1120. DOI:10.1029/2002GL016356
- Kleeman R, McCreary JP and Klinger BA (1999) A mechanism for generating ENSO decadal variability. *Geophys Res Lett* 26:1743-1746
- Knutson TR and Manabe S (1998) Model assessment of decadal variability and trends in the tropical Pacific Ocean. *J Climate* 11:2273-2296
- Kramer MA (1991) Nonlinear principal component analysis using autoassociative neural networks. *AIChE J* 37:233-243

- Latif M, and Barnett TP (1996) Decadal climate variability over the North Pacific and North America: Dynamics and predictability. *J Climate* 9:2407-2423
- Li S, Hsieh WW and Wu A (2005) Hybrid coupled modeling of the tropical Pacific using neural networks. *J Geophys Res (Oceans)* (accepted)
- McPhaden MJ and Zhang D (2004) Pacific Ocean circulation rebounds, *Geophys Res Lett* 31:L18301. DOI:10.1029/2004GL020727
- Rodgers KB, Friederichs P and Latif M (2004) Tropical Pacific decadal variability and its relation to decadal modulations of ENSO. *J Climate* 17:3761-3774
- Smith TM and Reynolds RW (2004) Improved extended reconstruction of SST (1854-1997). *J Climate* 17:2466-2477
- Tang B (1995) Periods of linear development of the ENSO cycle and POP forecast experiments. *J Climate* 8:682-691
- Tang Y and Hsieh WW (2002) Hybrid coupled models of the tropical Pacific – ENSO prediction. *Clim Dynam* 19:343-353
- Thompson CJ and Battisti DS (2001) A linear stochastic dynamical model of ENSO. Part II: Analysis. *J. Climate* 14:445-466
- Tziperman E, Zebiak SE and Cane MA (1997) Mechanisms of Seasonal - ENSO interaction. *J Atmos Sci* 54(1):61-71
- Wang B and An S-I (2001) Why the properties of El Niño changed during the late 1970s. *Geophys Res Lett* 28:3709-3712.

- Wang B and An S-I (2002) A mechanism for decadal changes of ENSO behavior: Roles of background wind changes. *Clim Dynam* 18:475-486. DOI 10.1007/s00382-001-0189-5
- Wu A and Hsieh WW (2003) Nonlinear interdecadal changes of the El Niño-Southern Oscillation. *Clim Dynam* 21:719-730. DOI 10.1007/s00382-003-0361-1
- Zebiak SE and Cane MA (1987) A model El Niño-Southern Oscillation. *Mon Weather Review* 115:2262-2278
- Zhang R-H, Kleeman R, Zebiak SE, Keenlyside N and Raynaud S (2005) An empirical parameterization of subsurface entrainment temperature for improved SST anomaly simulations in an intermediate ocean model. *J Climate* 18:350-371
- Zhang Y, Wallace JM and Battisti DS (1997) ENSO-like interdecadal variability: 1900-93. *J Climate* 10:1004-1020
- Zwiers FW and von Storch H (1995) Taking serial correlation into account in tests of the mean. *J Climate* 8:336-351

Exp.	El Niño		La Niña	
	SST	WSx	SST	WSx
A	11	11	0	0
B	6	11	0	0
C	6	6	0	0
D	0	11	0	0
E	-11	-11	0	0

Table 1: The eastward shift (in degrees longitude) of the SST and zonal WS anomaly centers in the post-shift (1981-1995 for A, B, C, D; 1998-2003 for E) regime relative to the pre-shift (1961-1975 for A, B, C, D; 1992-1998 for E) regime during strong El Niño and strong La Niña, as determined from NLPCA. In set A, atmospheric and oceanic monthly climatology were prescribed for both regimes, in B only the atmospheric, and in C only the oceanic. See text for set D and E. The quantized nature of the shift values arose from the model atmospheric zonal grid being 5.625° .

Figure captions

Fig. 1 A schematic diagram illustrating the NN model for performing the NLPCA. The model is a standard feedforward NN (i.e. multi-layer perceptron), with 3 ‘hidden’ layers of variables or ‘neurons’ (denoted by circles) sandwiched between the input layer \mathbf{x} on the left and the output layer \mathbf{x}' on the right. Next to the input layer is the encoding layer, followed by the ‘bottleneck’ layer with a single neuron u , then the decoding layer, and finally the output layer, i.e. a total of 4 layers of transfer functions are needed to map from the inputs to the outputs. A neuron v_i at the i th layer receives its value from the neurons \mathbf{v}_{i-1} in the preceding layer, i.e. $v_i = f_i(\mathbf{w}_i \cdot \mathbf{v}_{i-1} + b)$, where \mathbf{w}_i is a vector of weight parameters and b a bias parameter, and the transfer functions f_1 and f_3 are the hyperbolic tangent functions, while f_2 and f_4 are simply the identity functions. Effectively, a nonlinear function $u = F(\mathbf{x})$ maps from the higher dimension input space to the lower dimension bottleneck space, followed by an inverse transform $\mathbf{x}' = \mathbf{G}(u)$ mapping from the bottleneck space back to the original space, as represented by the outputs. To make the outputs as close to the inputs as possible, the cost function $J = \langle \|\mathbf{x} - \mathbf{x}'\|^2 \rangle$ (i.e. the mean square error, MSE) is minimized. Through the optimization, the values of the weight and bias parameters are solved. Data compression is achieved by the bottleneck, yielding the nonlinear principal component (NLPC) u . See Hsieh (2004) for details.

Fig. 2 Relations between PC1 of the T_{sub} anomalies and (a) PC1 and (b) PC2 of the h anomalies, as found by nonlinear regression via neural networks (overlapping circles), and linear regression (dashed lines), with the data shown as dots. The corresponding relations for PC2 of the T_{sub} anomalies are shown in (c) and (d).

Fig. 3 The decadal differences in the (a) SST ($^{\circ}\text{C}$) and (b) the WS (dyn cm^{-2}) over the tropical

Pacific. Shaded regions indicate 5% significance by the corrected t test (Zwiers and Von Storch, 1995).

Fig. 4 The observed zonal wind stress WS_x (dyn cm^{-2}) anomaly patterns from the leading NLPCA mode for the 1961-1975 regime ((a) and (b)) and for the 1981-1995 regime ((c) and (d)), with panels in the left column showing the anomalies when the NLPC u assumes its maximum value (i.e. during strong El Niño), and the right column, the minimum value (strong La Niña). Regions with values greater than 0.1 dyn cm^{-2} or less than -0.1 dyn cm^{-2} are shaded. “L” and “H” mark the location of the lowest and highest values, respectively.

Fig. 5 The net shortwave radiation flux (W m^{-2}) anomaly pattern (left column) and latent heat flux (W m^{-2}) anomaly pattern (right column) at the sea surface from the leading NLPCA mode in the 1961-1975 regime ((a)-(d)) and in the 1979-1993 regime ((e)-(h)) when the NLPC u assumes its maximum value (strong El Niño) and minimum value (strong La Niña). Regions with values greater than 10 W m^{-2} or less than -10 W m^{-2} are shaded. “L” and “H” mark the location of the lowest and highest values, respectively.

Fig. 6 Set A experiments using the climatology of the oceanic and the atmospheric fields for the 1961-1975 regime ((a)-(d)) and for the 1981-1995 regime ((e)-(h)) : The SST anomaly pattern (left column) and zonal WS anomaly pattern (right column) from the leading NLPCA mode when the NLPC takes its maximum value (strong El Niño) and minimum value (strong La Niña). Regions with anomaly magnitude exceeding $1.0 \text{ }^\circ\text{C}$ or 0.2 dyn cm^{-2} are shaded. “L” and “H” mark the location of the lowest and highest values, respectively.

Fig. 7 The model convergence heating rate field Q_c (m^2s^{-3}) from the leading NLPCA mode when the NLPC takes its maximum value (i.e. strong El Niño) when the (a) 1961-1975 and (b) 1981-1995 climatologies were used. Regions with anomaly magnitude exceeding $0.01 \text{ m}^2\text{s}^{-3}$

are shaded.

Fig. 8 Potential predictability of the Niño 3.4 SST anomaly index, as given by the cross-validated correlation between the predicted and actual index in the coupled model using climatologies from the pre-shift and post-shift regimes. Cross-validation was performed by dividing the 150 years into five segments, where for each segment chosen to test the forecast correlation skills, the other four were used to build the forecast models.

Fig. 9 Spectrum of the Niño 3.4 SST anomaly index in the coupled model using climatologies from the pre-shift regime (solid curve) and post-shift regime (dashed curve).

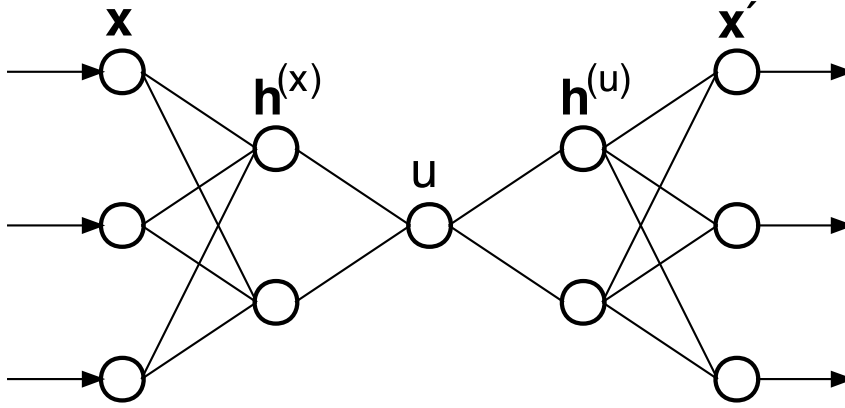


Figure 1: A schematic diagram illustrating the NN model for performing the NLPCA. The model is a standard feedforward NN (i.e. multi-layer perceptron), with 3 ‘hidden’ layers of variables or ‘neurons’ (denoted by circles) sandwiched between the input layer \mathbf{x} on the left and the output layer \mathbf{x}' on the right. Next to the input layer is the encoding layer, followed by the ‘bottleneck’ layer with a single neuron u , then the decoding layer, and finally the output layer, i.e. a total of 4 layers of transfer functions are needed to map from the inputs to the outputs. A neuron v_i at the i th layer receives its value from the neurons \mathbf{v}_{i-1} in the preceding layer, i.e. $v_i = f_i(\mathbf{w}_i \cdot \mathbf{v}_{i-1} + b)$, where \mathbf{w}_i is a vector of weight parameters and b a bias parameter, and the transfer functions f_1 and f_3 are the hyperbolic tangent functions, while f_2 and f_4 are simply the identity functions. Effectively, a nonlinear function $u = F(\mathbf{x})$ maps from the higher dimension input space to the lower dimension bottleneck space, followed by an inverse transform $\mathbf{x}' = \mathbf{G}(u)$ mapping from the bottleneck space back to the original space, as represented by the outputs. To make the outputs as close to the inputs as possible, the cost function $J = \langle \|\mathbf{x} - \mathbf{x}'\|^2 \rangle$ (i.e. the mean square error, MSE) is minimized. Through the optimization, the values of the weight and bias parameters are solved. Data compression is achieved by the bottleneck, yielding the nonlinear principal component (NLPC) u . See Hsieh (2004) for details.

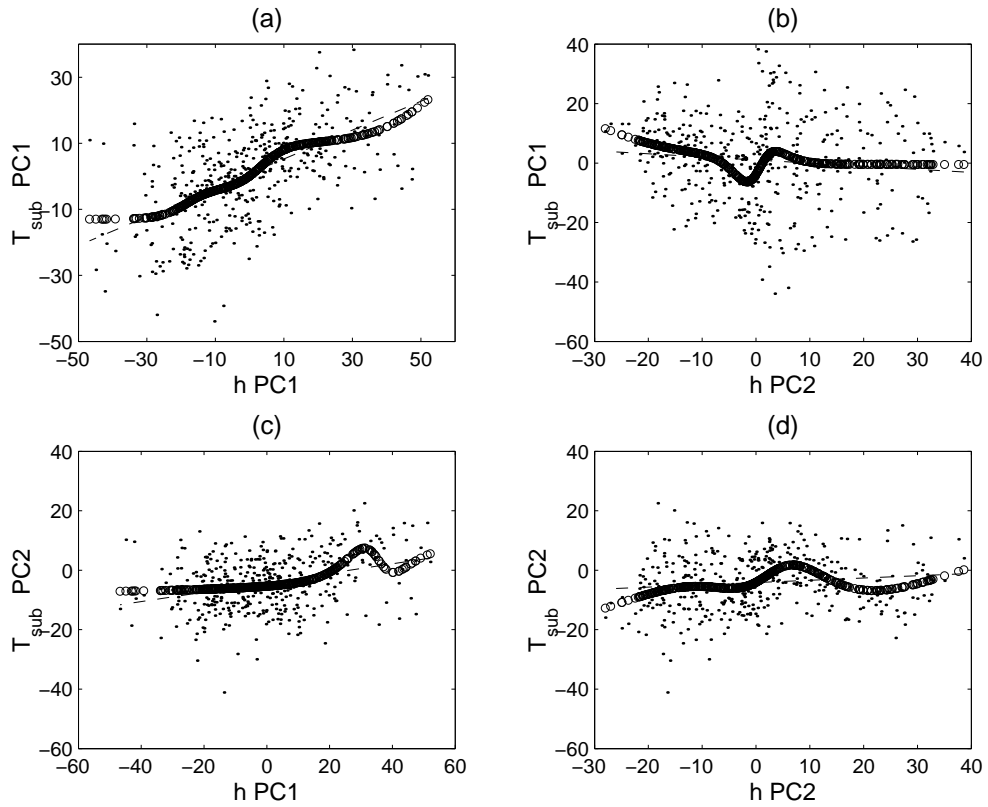
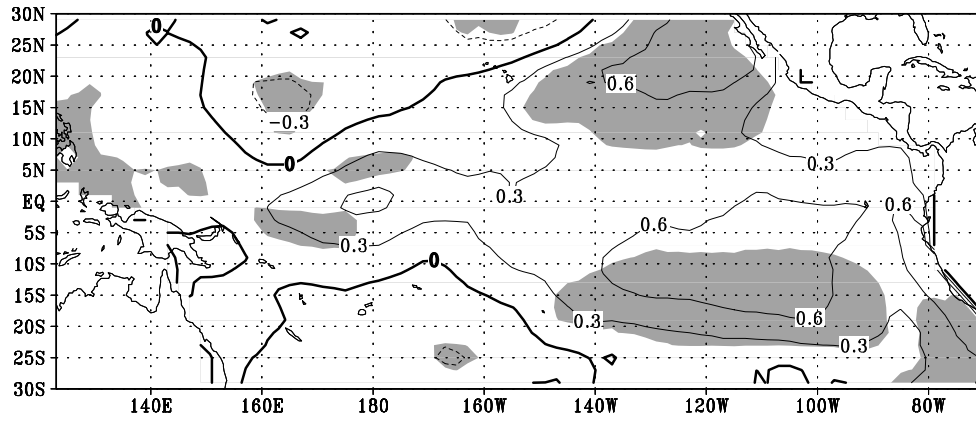


Figure 2: Relations between PC1 of the T_{sub} anomalies and (a) PC1 and (b) PC2 of the h anomalies, as found by nonlinear regression via neural networks (overlapping circles), and linear regression (dashed lines), with the data shown as dots. The corresponding relations for PC2 of the T_{sub} anomalies are shown in (c) and (d).

(a) SST difference (1981–1995 minus 1961–1975)



(b) WS difference (1981–1995 minus 1961–1975)

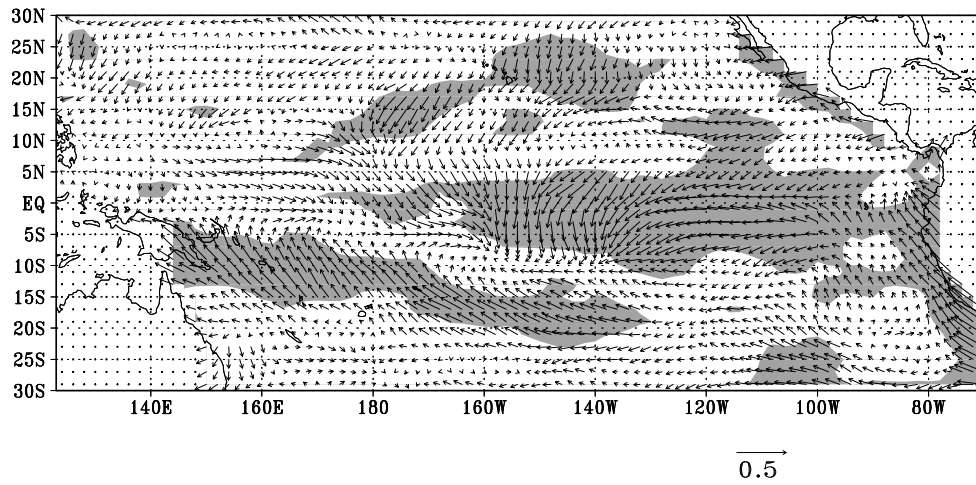


Figure 3: The decadal differences in the (a) SST ($^{\circ}\text{C}$) and (b) the WS (dyn cm^{-2}) over the tropical Pacific. Shaded regions indicate 5% significance by the corrected t test (Zwiers and Von Storch, 1995).

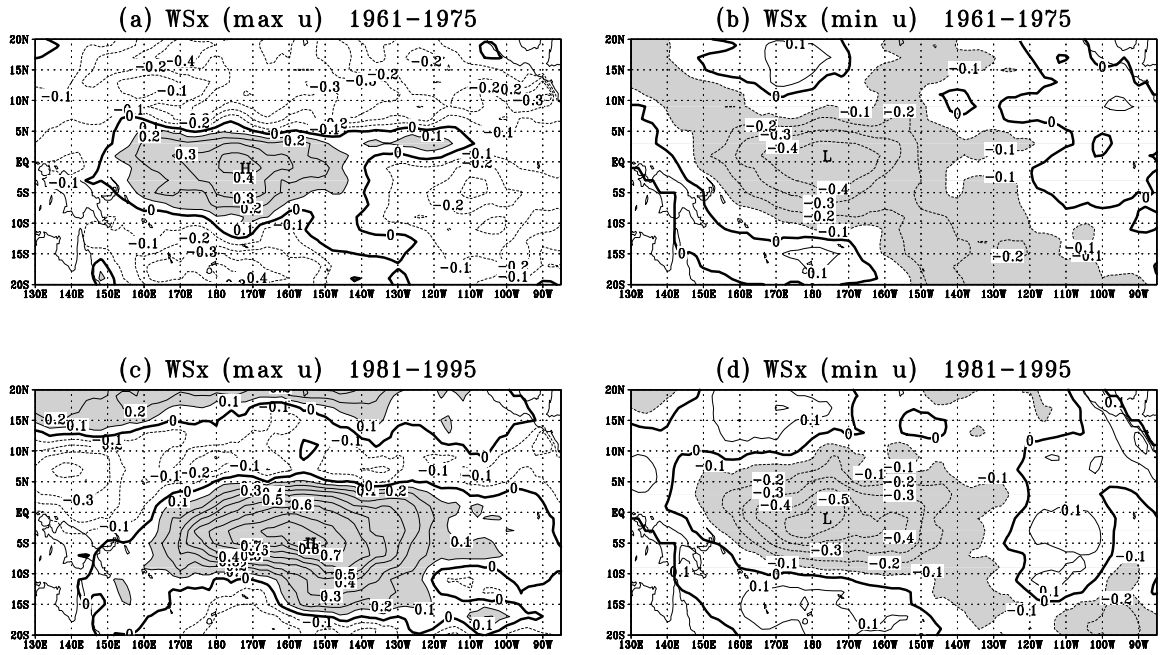


Figure 4: The observed zonal wind stress WSx (dyn cm^{-2}) anomaly patterns from the leading NLPCA mode for the 1961-1975 regime ((a) and (b)) and for the 1981-1995 regime ((c) and (d)), with panels in the left column showing the anomalies when the NLPC u assumes its maximum value (i.e. during strong El Niño), and the right column, the minimum value (strong La Niña). Regions with values greater than 0.1 dyn cm^{-2} or less than -0.1 dyn cm^{-2} are shaded. “L” and “H” mark the location of the lowest and highest values, respectively.

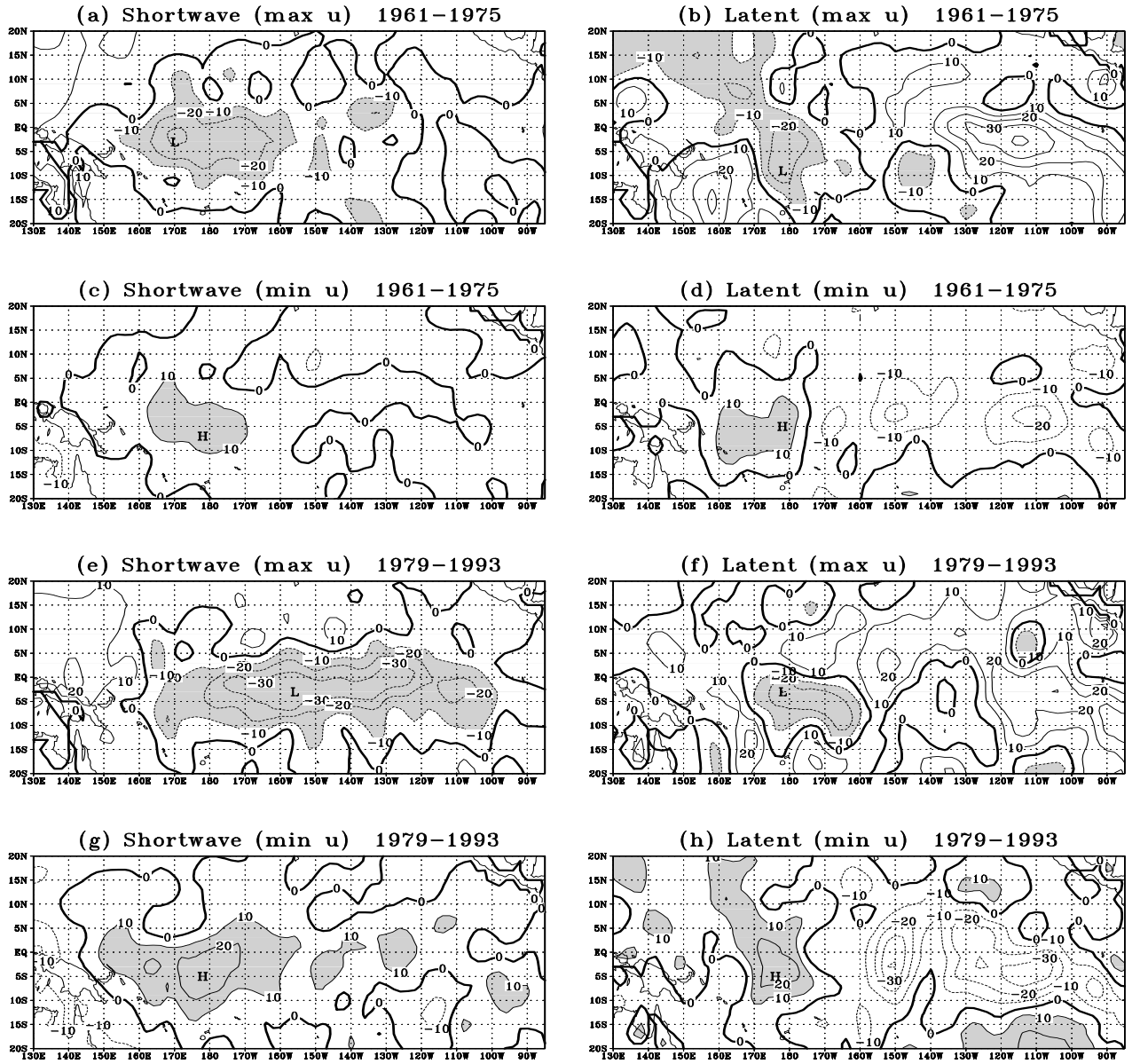


Figure 5: The net shortwave radiation flux (W m^{-2}) anomaly pattern (left column) and latent heat flux (W m^{-2}) anomaly pattern (right column) at the sea surface from the leading NLPKA mode in the 1961-1975 regime ((a)-(d)) and in the 1979-1993 regime ((e)-(h)) when the NLPK u assumes its maximum value (strong El Niño) and minimum value (strong La Niña). Regions with values greater than 10 W m^{-2} or less than -10 W m^{-2} are shaded. “L” and “H” mark the location of the lowest and highest values, respectively.

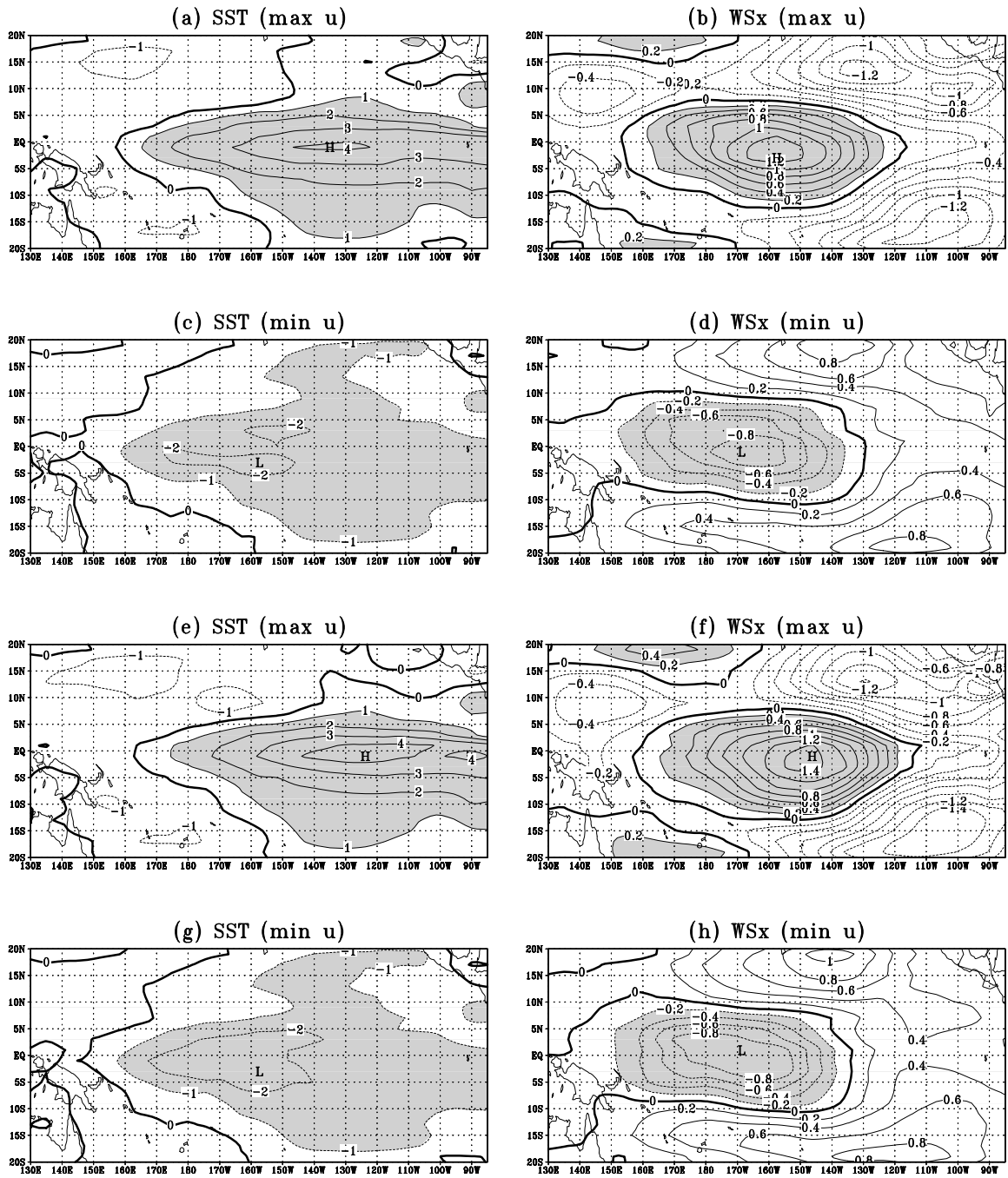


Figure 6: Set A experiments using the climatology of the oceanic and the atmospheric fields for the 1961-1975 regime ((a)-(d)) and for the 1981-1995 regime ((e)-(h)) : The SST anomaly pattern (left column) and zonal WS anomaly pattern (right column) from the leading NLPCA mode when the NLPC takes its maximum value (strong El Niño) and minimum value (strong La Niña). Regions with anomaly magnitude exceeding 1.0 °C or 0.2 dyn cm⁻² are shaded. “L” and “H” mark the location of the lowest and highest values, respectively.

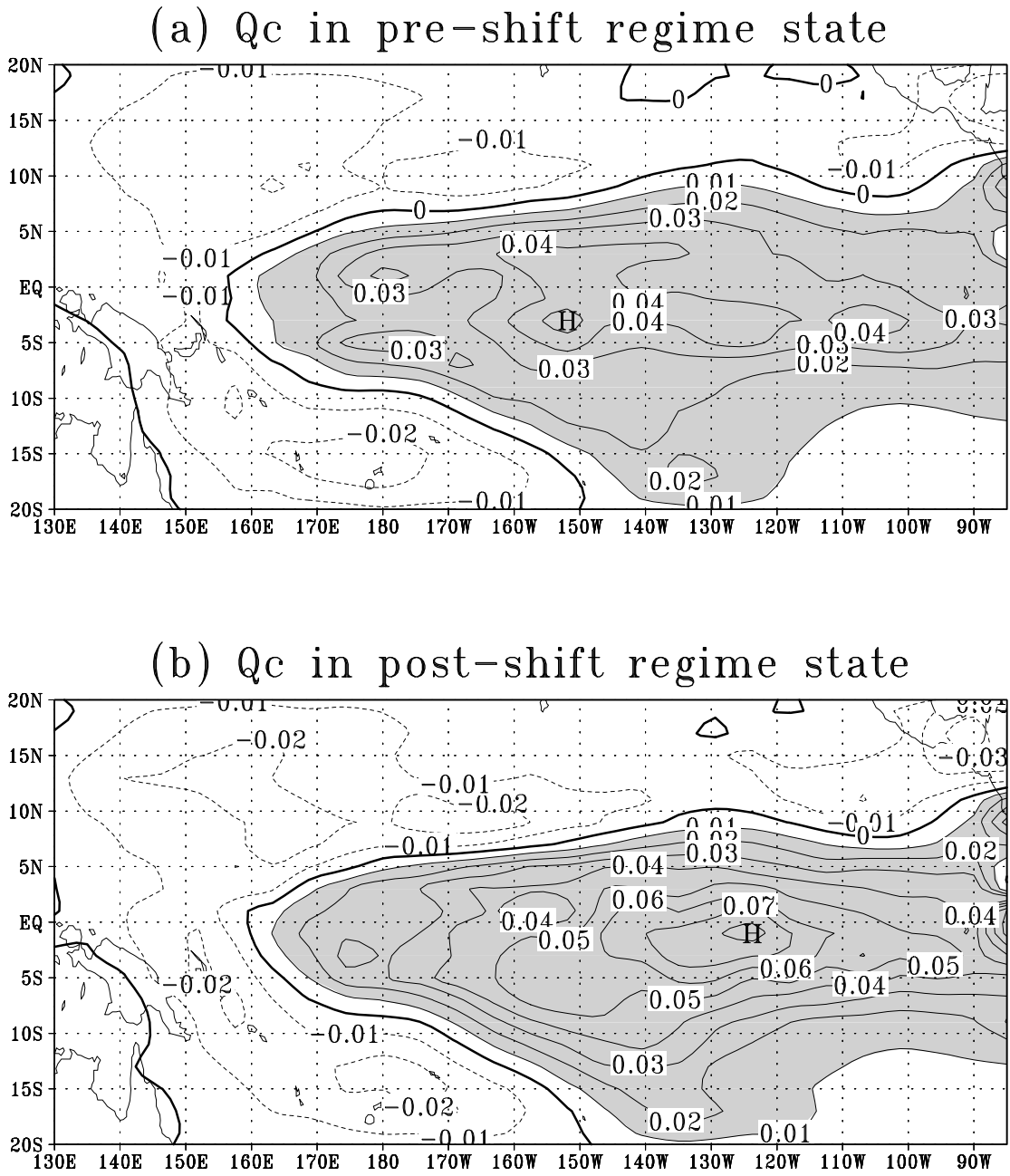


Figure 7: The model convergence heating rate field Q_c (m^2s^{-3}) from the leading NLPCA mode when the NLPC takes its maximum value (i.e. strong El Niño) when the (a) 1961-1975 and (b) 1981-1995 climatologies were used. Regions with anomaly magnitude exceeding $0.01 \text{ m}^2\text{s}^{-3}$ are shaded.

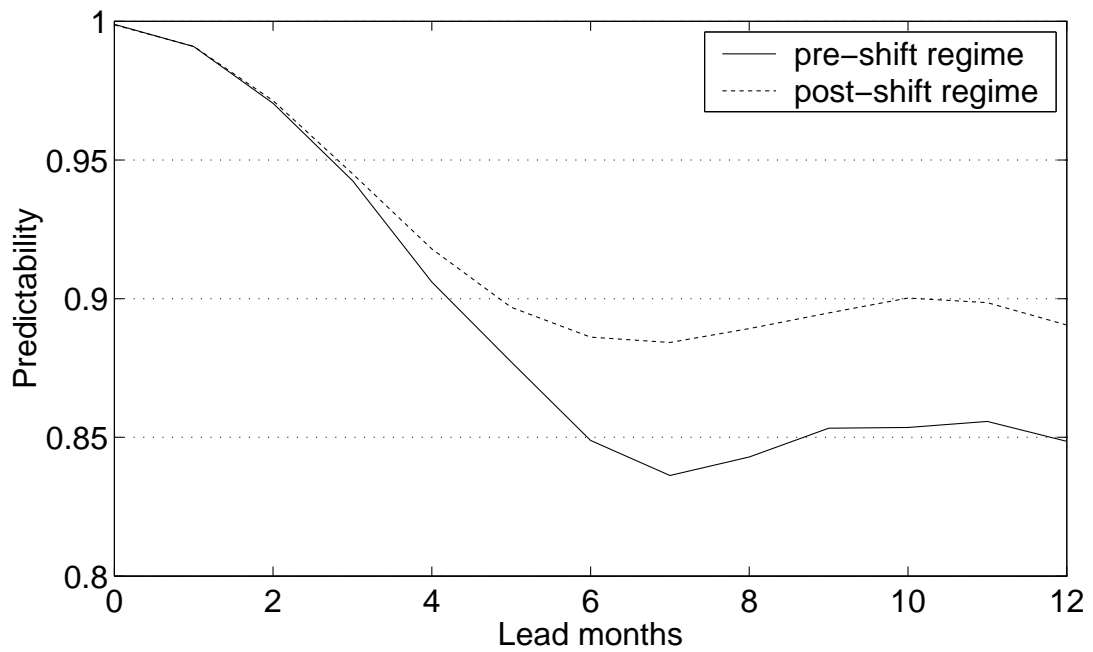


Figure 8: Potential predictability of the Niño 3.4 SST anomaly index, as given by the cross-validated correlation between the predicted and actual index in the coupled model using climatologies from the pre-shift and post-shift regimes. Cross-validation was performed by dividing the 150 years into five segments, where for each segment chosen to test the forecast correlation skills, the other four were used to build the forecast models.

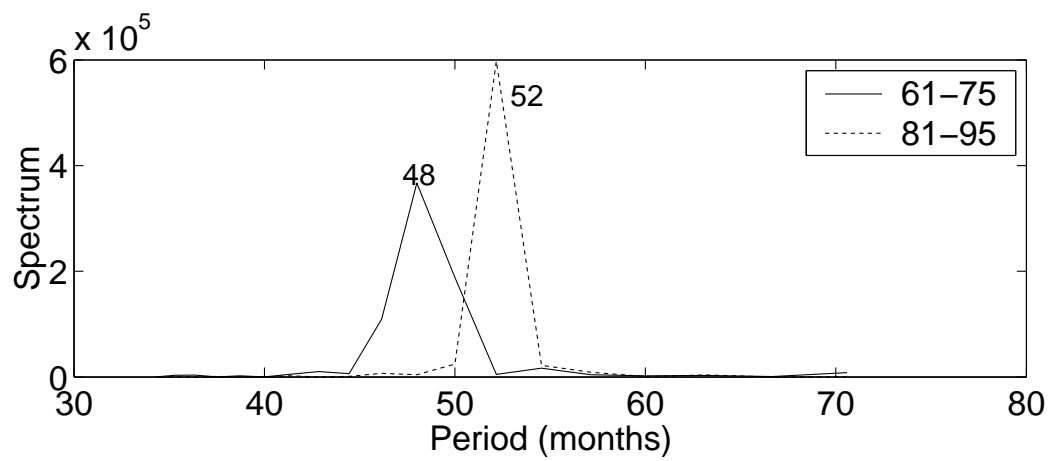


Figure 9: Spectrum of the Niño 3.4 SST anomaly index in the coupled model using climatologies from the pre-shift regime (solid curve) and post-shift regime (dashed curve).